

Measurement of the ZZ production cross section and limits on anomalous neutral triple gauge couplings in proton-proton collisions at $\sqrt{s} = 7$ TeV with the ATLAS detector

Shih-Chieh Hsu on behalf of ATLAS
 Lawrence Berkeley National Lab, Berkeley, CA, USA

A measurement of the ZZ production cross section in proton-proton collisions at $\sqrt{s} = 7$ TeV using data collected by the ATLAS experiment at the LHC is presented. In a data sample corresponding to an integrated luminosity of 1.02 fb^{-1} [1], 12 events containing two Z boson candidates decaying to electrons and/or muons were observed. The expected background contribution is $0.3_{-0.3}^{+0.9}(\text{stat})_{-0.3}^{+0.4}(\text{syst})$ events. The total cross section for on-shell ZZ production has been determined to be $\sigma_{ZZ}^{\text{tot}} = 8.4_{-2.3}^{+2.7}(\text{stat})_{-0.7}^{+0.4}(\text{syst}) \pm 0.3(\text{lumi}) \text{ pb}$ and is compatible with the Standard Model expectation of $6.5_{-0.2}^{+0.3} \text{ pb}$ calculated at the next-to-leading order in QCD. Limits on anomalous neutral triple gauge boson couplings are derived.

1. Introduction

The production of pairs of Z bosons at the LHC is of great interest since it provides a unique opportunity to test the predictions of the electroweak sector of the Standard Model at the TeV energy scale, and it is the irreducible background to the search for the Higgs boson in the $H \rightarrow ZZ$ decay channel or new phenomena beyond the SM [2, 3]. In the Standard Model, ZZ production proceeds via quark-antiquark t -channel annihilation; Figure 1 shows the leading-order Feynman diagrams for ZZ production from $q\bar{q}$ initial states. The ZZZ and $ZZ\gamma$ neutral triple gauge boson couplings (nTGCs) are zero in the Standard Model, hence there is no contribution from s -channel $q\bar{q}$ annihilation at tree level. At the one-loop level the contribution is $\mathcal{O}(10^{-4})$ [4]. Many models of physics beyond the Standard Model predict values of these couplings at the level of 10^{-4} to 10^{-3} [5]. Most non-zero values of ZZZ and $ZZ\gamma$ couplings increase the ZZ cross section at high ZZ invariant mass and high transverse momentum of the Z bosons [6]. ZZ production has been studied in e^+e^- collisions at LEP [7–11] and in antiproton-proton collisions at the Tevatron [12–15]. No deviation of the measured cross section from Standard Model expectation has been observed, allowing limits on anomalous nTGCs to be set [11, 13].

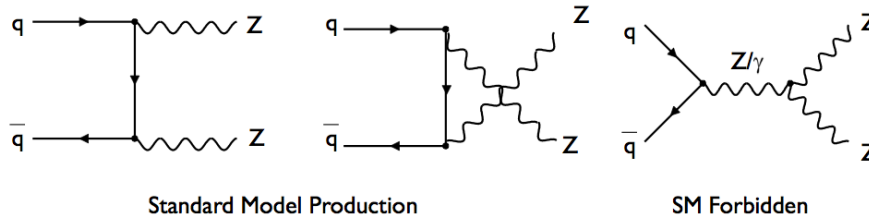


Figure 1: Tree-level Feynman diagrams for ZZ production through the $q\bar{q}$ initial state in hadron colliders. The s -channel diagram, on the right, contains the ZZZ ($ZZ\gamma$) neutral triple gauge boson coupling vertex, which is zero in the Standard Model.

This paper presents the first measurement of ZZ^1 production in proton-proton collisions at a centre-of-mass energy \sqrt{s} of 7 TeV, and limits on the anomalous nTGCs [16]. The measurement uses a data sample corresponding to an integrated luminosity of 1.02 fb^{-1} collected by the ATLAS detector at the LHC between February and June 2011. The cross section for on-shell ZZ production is predicted at next-to-leading order in QCD (NLO) to be $6.5_{-0.2}^{+0.3} \text{ pb}$; this includes a $\sim 6\%$ contribution from gluon fusion [17]. Candidate ZZ events are reconstructed in the $ZZ \rightarrow \ell^+\ell^-\ell^+\ell^-$ decay channel, where ℓ can be an electron or muon. Although this channel constitutes only $\sim 0.5\%$ of the total on-shell ZZ cross section, the expected signal to background ratio of four high transverse-momentum and isolated leptons is ~ 30 .

To reduce systematic uncertainties the cross section is measured within a phase-space that corresponds closely to the experimental selection cuts, namely requiring the mass of both lepton pairs to be between 66 GeV and

¹Throughout this paper Z should be taken to mean Z/γ^* .

116 GeV and all four leptons to be within the pseudorapidity² range $|\eta| < 2.5$ and have transverse momentum (p_T) greater than 15 GeV. This is termed the ‘fiducial’ cross section. The total ZZ cross section in the on-shell approximation is obtained from the fiducial cross section using the known $Z \rightarrow \ell^+\ell^-$ branching ratio and a correction factor for the kinematic and geometrical acceptance.

Anomalous nTGCs for on-shell ZZ production can be parameterized by two CP-violating (f_4^V) and two CP-conserving (f_5^V) complex parameters ($V = Z, \gamma$) which are zero in the Standard Model [6]. To ensure the partial-wave unitarity, a form-factor parameterization is introduced to cause the couplings to vanish at high center-of-mass energy $\sqrt{\hat{s}}$: $f_i^V = f_{i0}^V/(1 + \hat{s}/\Lambda^2)^n$. Here, Λ is the energy scale at which physics beyond the Standard Model will be directly observable, f_{i0}^V are the low-energy approximations of the couplings, and n is the form-factor power. Following Ref. [6], we set $n = 3$ and the form-factor scale Λ to 2 TeV, so that expected limits are within the values provided by unitarity at LHC energies. The results with energy cutoff $\Lambda = \infty$ are also presented as a comparison in the unitarity violation scheme.

2. Detector, Data and Monte Carlo Simulation

The ATLAS detector [18] consists of an inner tracking detector surrounded by a superconducting solenoid, electromagnetic and hadronic calorimeters and a muon spectrometer with a toroidal magnetic field. The inner detector, in combination with the 2 T magnetic field from the solenoid, provides precision tracking of charged particles for $|\eta| < 2.5$. It consists of a silicon pixel detector, a silicon strip detector and a straw tube tracker that also produces transition radiation measurements for electron identification. The calorimeter system covers the pseudorapidity range $|\eta| < 4.9$. It is composed of sampling calorimeters with either liquid argon (LAr) or scintillating tiles as the active media. In the region $|\eta| < 2.5$ the electromagnetic LAr calorimeter is finely segmented and plays an important role in electron identification. The muon spectrometer has separate trigger and high-precision tracking chambers which provide muon identification in $|\eta| < 2.7$. A three-level trigger system selects events to record for offline analysis. The events in this analysis were selected with single-lepton triggers with transverse momentum thresholds of 20 GeV for electrons and 18 GeV for muons.

This measurement uses a data sample of proton-proton collisions at $\sqrt{s} = 7$ TeV recorded between February and June 2011. Data periods flagged with data quality problems that affect the lepton reconstruction are removed. After data quality cuts, the total integrated luminosity used in the analysis is 1.02 fb^{-1} . The luminosity uncertainty is 3.7% [1].

The signal acceptance is determined from a detailed Monte Carlo simulation. The leading order (LO) generator PYTHIA [19] with the MRST modified LO Parton Density Function (PDF) set [20] is used to model $pp \rightarrow ZZ \rightarrow \ell^+\ell^-\ell^+\ell^-$ events, where ℓ includes electrons, muons and tau leptons. The PYTHIA simulation includes the interference terms between the Z and γ^* diagrams. The minimum invariant mass generated for each Z/γ boson is set to 12 GeV. When calculating the expected number of signal events, the predictions of PYTHIA are normalized to the NLO calculation of MCFM [17] using the MSTW2008 [21] NLO PDF set. The normalization factor, calculated within the phase-space of our fiducial cross section measurement, is 1.44.

Background processes are estimated from the data and are cross-checked with predictions from Monte Carlo simulations. MC@NLO [22] is used to model the diboson processes W^+W^- and $W^\pm Z$, $t\bar{t}$ and single top-quark events, and MADGRAPH [23] is used for the $W/Z + \gamma$ final state. W^\pm or Z gauge bosons produced in association with jets are modelled with ALPGEN [24], except for those with a τ lepton in the final state where PYTHIA was used. Events with dileptons from Drell-Yan ($10 \text{ GeV} < m_{\ell^+\ell^-} < 40 \text{ GeV}$) production are also modelled with ALPGEN or PYTHIA, depending on the presence of τ leptons in the final state. Events with heavy flavour dijets are modelled with PYTHIAB [25].

Detector response is simulated [26] with a program based on GEANT4 [27]. The luminosity in a single bunch-crossing is high enough to produce several pp collisions per bunch crossing, the mean number typically being 6–8. Additional inelastic pp events are included in the simulation, distributed so as to reproduce the expected number of collisions per bunch-crossing in the data.

²ATLAS uses a right-handed coordinate system with its origin at the nominal interaction point in the centre of the detector and the z -axis along the beam pipe. The x -axis points from the interaction point to the centre of the LHC ring, and the y -axis points upwards. Cylindrical coordinates (r, ϕ) are used in the transverse plane, ϕ being the azimuthal angle around the beam pipe. The pseudorapidity η is defined in terms of the polar angle θ as $\eta = -\ln \tan(\theta/2)$.

3. Event selection, signal acceptance and efficiency

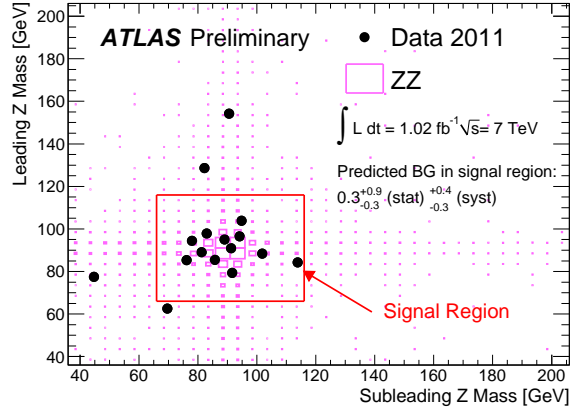


Figure 2: The mass of the leading (higher lepton pair p_T) Z candidate versus the mass of the subleading (lower lepton pair p_T) Z candidate. The events observed in the data are shown as solid circles and the signal prediction from simulation as pink boxes. The red box indicates the signal region defined by the cuts on the Z candidate masses.

In order to remove non-collision background, events are required to contain at least one vertex formed from at least three good tracks. The vertex with the largest sum of the p_T^2 computed with the associated tracks is selected as the primary vertex. Signal events are characterized by four high- p_T , isolated electrons or muons, in three channels: $e^+e^-e^+e^-$, $\mu^+\mu^-\mu^+\mu^-$ and $e^+e^-\mu^+\mu^-$. Lepton candidates are required to be consistent with originating from the primary vertex.

Electrons are reconstructed from a cluster in the electromagnetic calorimeter matched to a track in the inner detector [28]. Electron candidates are required to have a transverse energy (measured in the calorimeter) of at least 15 GeV and a pseudorapidity of $|\eta| < 2.47$. They must be isolated, using the same criterion as for muons, calculating the Σp_T around the electron track. Electron candidates within $\Delta R = 0.1$ of any selected muon are rejected, and if two electron candidates are within $\Delta R = 0.1$ of each other the one with the lower p_T is rejected. The overall reconstruction and identification efficiency varies as a function of p_T from 63% at 15 GeV to 81% at 45 GeV.

Muons are identified by matching tracks (or track segments) reconstructed in the muon spectrometer to tracks reconstructed in the inner detector [28]. Their momentum is calculated by combining the information from the two subsystems and correcting for the energy lost in the calorimeter. Only muons with $p_T > 15$ GeV and $|\eta| < 2.5$ are considered. In order to reject muons from the decay of heavy quarks, isolated muons are selected, by requiring the scalar sum of the transverse momenta (Σp_T) of other tracks inside a cone of $\Delta R \equiv \sqrt{\Delta\phi^2 + \Delta\eta^2} = 0.2$ around the muon to be no more than 15% of the muon p_T . The muon reconstruction and isolation efficiencies were measured in data, using a tag-and-probe technique on a large sample of $Z \rightarrow \mu^+\mu^-$ events. The overall reconstruction and identification efficiency varies as a function of p_T from 92% at 15 GeV to 95% at 45 GeV.

Selected events are required to have exactly four leptons selected as above, and to have passed a single-muon or single-electron trigger. To ensure event selection at trigger efficiency plateau, at least one of these leptons must have $p_T > 20$ GeV (25 GeV) for a muon (electron) and match to an object of the same flavor reconstructed online by the trigger system within $\Delta R < 0.1$ (0.15).

Same-flavour, oppositely-charged lepton pairs are combined to form Z candidates. An event must contain two such pairs. In the $e^+e^-e^+e^-$ and $\mu^+\mu^-\mu^+\mu^-$ channels, ambiguities are resolved by choosing the pairing which results in the smaller value of the sum of the two $|m_{\ell^+\ell^-} - m_Z|$ values. Figure 2 shows a scatter plot of the invariant mass of the leading (higher lepton pair p_T) lepton pair against that of the subleading (lower lepton pair p_T) lepton pair. The events cluster in the region where both masses are around m_Z , with some contribution from events with one Z boson off-shell. Events are required to contain two Z candidates with invariant masses satisfying $66 \text{ GeV} < m_{\ell^+\ell^-} < 116 \text{ GeV}$.

The reconstruction efficiency for the ZZ candidates, including the trigger efficiency, the lepton identification and reconstruction efficiencies is derived from simulation. It is corrected with scale factors to account for small differences in efficiencies between data and simulation.

The efficiencies of the single-lepton triggers have been determined as a function of lepton p_T using large samples of single $Z \rightarrow \ell^+\ell^-$ events. The trigger efficiencies for the four-lepton events passing the offline selections are obtained from simulation, corrected by scale factors derived from the comparison between data and Monte Carlo of the single lepton trigger efficiencies, and are found to be close to 100% with uncertainty 0.04%.

For lepton reconstruction and identification, the scale factors vary from unity by 1%–13% for electrons and 0.1%–2% for muons [29] depending on the p_T . The larger discrepancies seen for electrons affect only the low- p_T region, and are due to mis-modelling of lateral shower shapes in simulation. Systematic uncertainties on these scale factors are derived from efficiency measurements in the data. A $\sim 1\%$ correction is applied to the calorimeter energy scale and resolution for electron so that the $Z \rightarrow e^+e^-$ invariant mass distribution in data is correctly reproduced by the simulation; similarly, a small correction (1% at 15 GeV–2% at 50 GeV) is applied to muon p_T .

The performance of the Monte Carlo simulation relative to the data has been checked using single Z boson candidates. Same-flavour opposite-sign lepton pairs were selected using the criteria above, including the trigger requirement, and compared to simulation after applying all corrections. The invariant mass distributions of dimuon and dielectron pairs are shown in Fig. 3(a) and (b) respectively; reasonable agreement is seen.

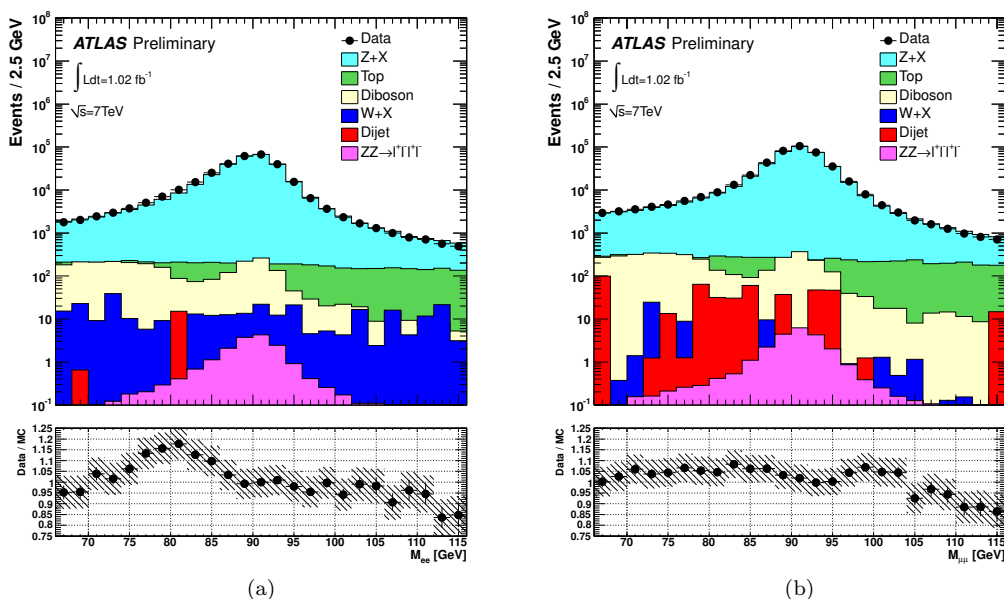


Figure 3: Invariant mass of (a) dielectron Z candidates and (b) dimuon Z candidates. The different background sources are shown in different colours. The ratio between data and Monte Carlo is shown in the lower part of each histogram; the total error (statistical plus systematic) is indicated by the shaded band. Diboson includes WW , WZ , $W\gamma$ and $Z\gamma$.

The overall efficiencies of the reconstruction and selection criteria for events generated within the fiducial phase-space are $41\pm 3\%$, $81\pm 2\%$, $57\pm 2\%$ and $59\pm 2\%$ for $e^+e^-e^+e^-$, $\mu^+\mu^-\mu^+\mu^-$, $e^+e^-\mu^+\mu^-$ and $\ell^+\ell^-\ell^+\ell^-$ respectively. They include contributions of 1.6% from $ZZ \rightarrow \ell^+\ell^-\ell^+\ell^-$ events generated outside the fiducial phase-space and 0.3% from events where one of the Z bosons decays to tau leptons. The lower signal expectation in the $e^+e^-e^+e^-$ channel compared with the $\mu^+\mu^-\mu^+\mu^-$ channel reflects the lower electron identification efficiency. The dominant systematic uncertainties arise from electron identification (6.6% in the $e^+e^-e^+e^-$ final state, 3.1% in the $e^+e^-\mu^+\mu^-$ final state) and from the muon reconstruction efficiency (2.0% in $\mu^+\mu^-\mu^+\mu^-$ and 1.0% in $e^+e^-\mu^+\mu^-$).

4. Background Estimation

Background to the ZZ signal originates from events with a Z (or W^\pm) boson decaying to leptons plus additional jets or photons ($W/Z + X$) and from top-quark pair-production ($t\bar{t}$) or single-top production. The jets may be misidentified as electrons or contain electrons or muons from in-flight decays of pions, kaons, or heavy-flavoured hadrons; photons may be misidentified as electrons. The majority of these background leptons

are rejected by the isolation requirement, but some may satisfy the isolation cuts. Since Monte Carlo simulations may not model well the jet fragmentation in the tails of the isolation distributions, the background is estimated directly from the data.

To estimate the background contribution from four-lepton events in which one lepton does not originate from the decay of a Z boson but from a jet, a sample of events in the data containing three leptons passing all selection criteria plus one ‘lepton-like jet’ is identified; such events are denoted $\ell\ell j$. For muons, the lepton-like jets are muon candidates that fail the isolation requirement. For electrons, the lepton-like jets are clusters in the electromagnetic calorimeter matched to inner detector tracks that fail either or both of the full electron selection and the isolation requirement. The events are otherwise required to pass the full event selection, treating the lepton-like jet as if it were a fully identified lepton. This event sample is dominated by $Z + X$ events. The background is then estimated by scaling this control sample by a measured factor f (η and p_T dependent, treated as uncorrelated in the two variables) which is the ratio of the probability for a jet to satisfy the full lepton criteria to the probability to satisfy the lepton-like jet criteria. The background in which two selected leptons originate from a jet is treated similarly, by identifying a data sample with two leptons and two lepton-like jets; such events are denoted $\ell\ell j j$. To avoid double counting in the background estimate, and to take account of the expected ZZ contribution, the total number of background events is calculated as:

$$N(\text{background}) = N(\ell\ell j) \times f - N(\ell\ell j j) \times f^2 - N(ZZ \text{ in control region}). \quad (1)$$

The factor f is measured in a sample of data selected with single-lepton triggers with cuts applied to suppress isolated leptons from W^\pm and Z bosons, and corrected for the remaining small contribution of true leptons using simulation. A similar analysis is performed on Monte Carlo simulation; the larger of the statistical error on f determined from the data and the difference between data and simulation is taken as the systematic uncertainty in each p_T (or η) bin. This results in an average of systematic uncertainty of $\sim 30\%$ for each $p_T(\eta)$ bin except the lowest p_T (15 – 20 GeV) bin, for which there is a 100% systematic uncertainty.

5. Cross section measurement

The numbers of expected and observed events after applying all selection cuts are shown in Table I and depicted in Figure 4. The expected yields are compatible to theoretical predictions. We observe 12 ZZ candidates in data with a background expectation of $0.3_{-0.3}^{+0.9}$, corresponding to a p-value of 3.4×10^{-6} equivalent to a one-sided Gaussian significance of 4.5σ . In the four-muon channel 8 events are observed where only $3.3_{-0.5}^{+1.0}$ total signal plus background events are expected. The probability of the expected number fluctuating up to 8 or more is 6.4%.

Final State	$e^+e^-e^+e^-$	$\mu^+\mu^-\mu^+\mu^-$	$e^+e^-\mu^+\mu^-$	$\ell^+\ell^-\ell^+\ell^-$
Observed	2	8	2	12
Bkg(data-driven)	$0.01_{-0.01-0.01}^{+0.03+0.05}$	$0.3_{-0.3}^{+0.9} \pm 0.3$	$< 0.01_{-0.01}^{+0.03}$	$0.3_{-0.3-0.3}^{+0.9+0.4}$
Expected ZZ	$1.57 \pm 0.03 \pm 0.11$	$3.09 \pm 0.04 \pm 0.06$	$4.5 \pm 0.1 \pm 0.2$	$9.1 \pm 0.1 \pm 0.3$

Table I: Summary of observed events, total background contributions and expected signal in the individual four-lepton and combined channels. The first error is statistical while the second is systematic. The uncertainty on the luminosity is not included. The errors on the background estimates span the 68% confidence interval, which is not symmetric about the best estimate because the background cannot be negative.

The ZZ fiducial cross section was determined by maximizing a profile likelihood. The profile likelihood is derived by maximizing a likelihood including systematic uncertainties as nuisance parameters with respect to those nuisance parameters for each cross section value. The measured fiducial cross section is:

$$\sigma_{ZZ \rightarrow \ell^+\ell^-\ell^+\ell^-}^{\text{fid}} = 19_{-5}^{+6} \text{ (stat)} \quad {}_{-2}^{+1} \text{ (syst)} \quad \pm 1 \text{ (lumi)} \text{ fb}$$

where $\ell^+\ell^-\ell^+\ell^-$ refers to the sum of the $e^+e^-e^+e^-$, $e^+e^-\mu^+\mu^-$ and $\mu^+\mu^-e^+e^-$ final states. The total cross section was determined similarly, but correcting for the known $Z \rightarrow \ell^+\ell^-$ branching ratio and the acceptance of the fiducial cuts. The acceptance of the fiducial cuts, calculated at NLO using the program MCFM [17] version 6.0 with the MSTW2008 PDF set, is 0.507 ± 0.008 where the error arises from PDF uncertainties. The measured value of the total on-shell ZZ cross section is:

$$\sigma_{ZZ}^{\text{tot}} = 8.4_{-2.3}^{+2.7} \text{ (stat)} \quad {}_{-0.7}^{+0.4} \text{ (syst)} \quad \pm 0.3 \text{ (lumi)} \text{ pb.}$$

The result is statistically consistent with the NLO Standard Model total cross section for this process of $6.5_{-0.2}^{+0.3}$ pb, calculated with MCFM and parton density function set MSTW2008.

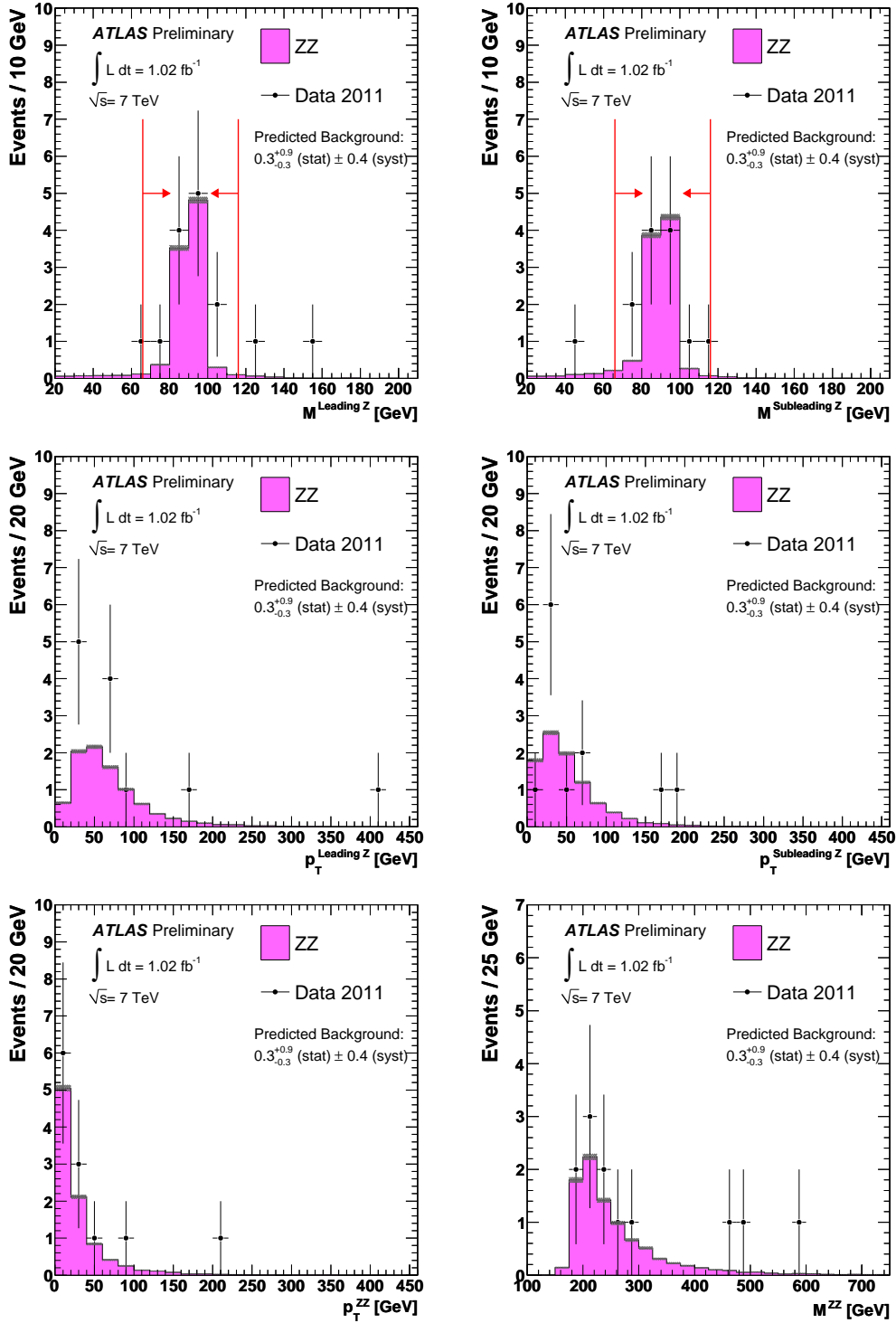


Figure 4: Kinematic distributions for ZZ candidates summed over all four-lepton channels. The top row shows the invariant mass of the leading (top left, higher lepton pair p_T) and subleading (top right, lower lepton pair p_T) lepton pair, after all cuts except on the variable plotted. The red bands indicate the signal region defined by the mass cut. The middle row shows the transverse momentum of the leading (middle left) and subleading (middle right) lepton pair, and the bottom row the transverse momentum p_T^{ZZ} (bottom left) and invariant mass M^{ZZ} (bottom right) of the four-lepton system, for selected candidates. The points represent the observed data and the histogram shows the signal prediction from simulation. The shaded band on the histogram shows the combined statistical and systematic uncertainty on the signal prediction. The predicted number of background events from the data-driven background estimate is indicated on the plot.

6. Limits on anomalous TGCs

Coupling 95% CI	f_4^γ	f_4^Z	f_5^γ	f_5^Z
$\Lambda = 2 \text{ TeV}$	$[-0.15, 0.15]$	$[-0.12, 0.12]$	$[-0.15, 0.15]$	$[-0.13, 0.13]$
$\Lambda = \infty$	$[-0.08, 0.08]$	$[-0.07, 0.07]$	$[-0.08, 0.08]$	$[-0.07, 0.07]$

Table II: One dimensional 95% confidence intervals for anomalous neutral gauge boson couplings, where the limit for each coupling assumes the other couplings fixed at their Standard Model value. A form factor scale of $\Lambda = 2 \text{ TeV}$ and ∞ are both presented. Limits were derived using both statistical and systematic uncertainties; the statistical uncertainties are dominant.

Limits on anomalous nTGCs are determined using the ZZ cross section. The cross section dependency on couplings is parametrized using fully simulated SHERPA [30] events subsequently reweighted using the leading order matrix element [6] within the framework of Bella [31] to account for the multidimensional dependence on acceptance and efficiencies. The reweighting procedure uses simulated samples with Standard Model as well as non-Standard Model coupling values to remove potential problems from large weights. One dimensional 95% confidence intervals on the anomalous nTGCs were determined using a maximum profile likelihood fit to the observed number of events. The systematic errors were included as nuisance parameters. The resulting limits for each coupling, determined assuming the other couplings fixed at their Standard Model value, are listed in Table II. The present limits are dominated by statistical uncertainties: limits derived using statistical uncertainties alone differ from those in Table II by less than 0.01. As shown in Figure 5, these limits are comparable with, or are more stringent than, those derived from measurements at LEP [11] and the Tevatron [13], although it should be noted that limits from LEP do not use a form factor, and those from the Tevatron use $\Lambda = 1.2 \text{ TeV}$.

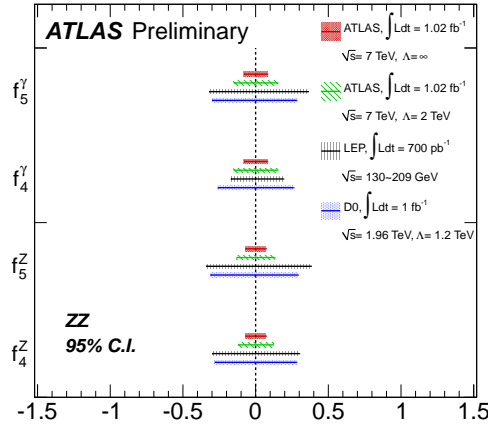


Figure 5: Anomalous nTGC 95% confidence intervals from ATLAS, LEP [11] and Tevatron [13] experiments. Luminosities, centre-of-mass energy and cut-off Λ for each experiment are shown.

7. Conclusion

The first measurement of the ZZ production cross-section in LHC proton-proton collisions at $\sqrt{s} = 7 \text{ TeV}$ has been performed by the ATLAS detector, using electrons and muons in the final state. In a dataset with an integrated luminosity of 1.02 fb^{-1} a total of 12 candidates was observed with a background expectation of $0.3_{-0.3}^{+0.9}(\text{stat})_{-0.3}^{+0.4}(\text{sys})$. The Standard Model expectation for the number of signal events is $9.1 \pm 0.1(\text{stat}) \pm 0.3(\text{sys})$. The fiducial and total cross sections were determined to be

$$\begin{aligned} \sigma_{ZZ \rightarrow \ell^+ \ell^- \ell^+ \ell^-}^{\text{fid}} &= 19_{-5}^{+6} (\text{stat}) \quad {}_{-2}^{+1} (\text{syst}) \pm 1 (\text{lumi}) \text{ fb} \\ \sigma_{ZZ}^{\text{tot}} &= 8.4_{-2.3}^{+2.7} (\text{stat}) \quad {}_{-0.7}^{+0.4} (\text{syst}) \pm 0.3 (\text{lumi}) \text{ pb}. \end{aligned}$$

The result is statistically consistent with the NLO Standard Model total cross section for this process of $6.5_{-0.2}^{+0.3}$ pb. 95% confidence intervals for anomalous neutral triple gauge boson couplings are derived which are compatible with zero, the value they have in the Standard Model. These limits are comparable with, or are more stringent than, those derived from measurements at LEP [11] and the Tevatron [13].

References

- 1 ATLAS Collaboration ATLAS-CONF-2011-116 (2011) .
- 2 K. Agashe et al. Phys. Rev. D 76 (2007) 036006.
- 3 L. Fitzpatrick et al. J. High Energy Phys. 0709 (2007) 013.
- 4 G. J. Gounaris, J. Layssac, and F. M. Renard Phys. Rev. D62 (2000) 073012.
- 5 J. Ellison and J. Wudka Annu. Rev. Nucl. Part. Sci. 48 (1998) 33.
- 6 U. Baur and D. L. Rainwater Phys. Rev. D62 (2000) 113011.
- 7 ALEPH Collaboration, R. Barate et al. Phys. Lett. B469 (1999) 287.
- 8 DELPHI Collaboration, J. Abdallah et al. Eur. Phys. J. C30 (2003) 447.
- 9 L3 Collaboration, M. Acciarri et al. Phys. Lett. B465 (1999) 363.
- 10 OPAL Collaboration, G. Abbiendi et al. Eur. Phys. J. C32 (2003) 303.
- 11 LEP Collaborations ALEPH, DELPHI, L3, OPAL, and the LEP Electroweak Working Group arXiv:hep-ex/0612034.
- 12 CDF Collaboration, T. Aaltonen et al. Phys. Rev. Lett. 100 (2008) 201801.
- 13 D0 Collaboration, V. M. Abazov et al. Phys. Rev. Lett. 100 (2008) 131801.
- 14 D0 Collaboration, V. M. Abazov et al. Phys. Rev. Lett. 101 (2008) 171803.
- 15 D0 Collaboration, V. M. Abazov et al. Phys. Rev. D84 (2011) 011103.
- 16 ATLAS Collaboration ATLAS-CONF-2011-107 (2011) .
- 17 J. M. Campbell, R. K. Ellis, and C. Williams J. High Energy Phys. 07 (2011) 018.
- 18 ATLAS Collaboration, G. Aad et al. JINST 3 (2008) S08003.
- 19 T. Sjostrand et al. Comput. Phys. Commun. 135 (2001) 238–259.
- 20 A. Sherstnev and R. S. Thorne Eur. Phys. J. C55 (2008) 553.
- 21 A. D. Martin, W. J. Stirling, R. S. Thorne, and G. Watt Eur. Phys. J. C63 (2009) 189.
- 22 S. Frixione and B.R. Webber J. High Energy Phys. 0206 (2002) 029.
- 23 J. Alwall et al. J. High Energy Phys. 09 (2007) 028.
- 24 M. L. Mangano, M. Moretti, F. Piccinini, R. Pittau, and A. Polosa J. High Energy Phys. 0307 (2003) .
- 25 S. P. Baranov and M. Smizanska Phys. Rev. D62 (2000) 014012.
- 26 ATLAS Collaboration, G. Aad et al. Eur.Phys.J. C70 (2010) 823–874.
- 27 S. Agostinelli et al. Nucl. Instrum. Meth. A 506 (2003) 250.
- 28 ATLAS Collaboration, G. Aad et al. J. High Energy Phys. 1012 (2010) 060.
- 29 ATLAS Collaboration ATLAS-CONF-2011-063 (2011) .
- 30 T. Gleisberg, S. Höche, F. Krauss, M. Schönherr, S. Schumann, F. Siegert, and J. Winter J. High Energy Phys. 02 (2009) 007.
- 31 G. Bella arXiv:0803.3307.